

# Matrix product solution of a left-permeable two-species asymmetric exclusion process

Arvind Ayyer <sup>\*a</sup>, Caley Finn <sup>†b</sup>, and Dipankar Roy <sup>‡a</sup>

<sup>a</sup>Department of Mathematics, Indian Institute of Science, Bangalore - 560012, India.

<sup>b</sup>LAPTh, CNRS - Université Savoie Mont Blanc, 9 chemin de Bellevue, BP 110, F-74941 Annecy-le-Vieux Cedex, France.

August 2017

## Abstract

We study a two-species partially asymmetric exclusion process where the left boundary is permeable for the ‘slower’ species but the right boundary is not. We find a matrix product solution for the stationary state, and the exact stationary phase diagram for the densities and currents. By calculating the density of each species at the boundaries, we find further structure in the stationary phases. In particular, we find that the slower species can reach and accumulate at the far boundary, even in phases where the bulk density of these particles approaches zero.

## 1 Introduction

Exclusion processes on finite lattices in contact with reservoirs are prototypical models of nonequilibrium statistical mechanics. Although these models are defined by simple dynamical rules, they exhibit rich phenomenology. Moreover, they have the property of being integrable, so that they can be analysed rigorously [1]. The simplest variant consists of a single type (or species) of particle and is called the Asymmetric Simple Exclusion Process (ASEP). When the asymmetry is total (resp. partial), it is called the TASEP (resp. PASEP). ASEPs with more than one kind of particle have found applications in recent times in biological [2, 3] and chemical [4] systems.

While the most general variant of the single-species ASEP has an integrable structure, this is no longer true even if there are two species of particles. In earlier work, progress has been made on understanding two-species exclusion process with boundaries.

---

\*Electronic address: [arvind@math.iisc.ernet.in](mailto:arvind@math.iisc.ernet.in)

†Corresponding author, Electronic address: [caley.finn@lapth.cnrs.fr](mailto:caley.finn@lapth.cnrs.fr)

‡Electronic address: [dipankar.roy15@math.iisc.ernet.in](mailto:dipankar.roy15@math.iisc.ernet.in)

Report number: LAPTH-029/17

Keywords: exclusion process, two species, phase diagram, left-permeable, matrix product algebra, Continuous big  $q$ -Hermite polynomials

Evans, Foster, Godr che and Mukamel showed that a special choice of boundary interactions exhibits spontaneous symmetry breaking [5]. Arita considered a semipermeable TASEP, where the slower species (also known as second-class particles) were trapped in the system, and determined the phase diagram [6]. Detailed properties of the phase diagram of this model were analysed by Ayyer, Lebowitz and Speer [7]. The latter also studied some two-species models whose phase diagram was determined using colouring techniques [8]. Uchiyama, in a remarkable paper, generalised the semipermeable TASEP to the semipermeable ASEP by using considerably more sophisticated techniques, and derived the phase diagram for the semipermeable PASEP [9]. More recently, integrable two-species models were classified by Crampe, Mallick, Ragoucy and Vanicat [10]. The detailed solution for one of the new integrable models discovered there was given by Crampe, Evans, Mallick, Ragoucy and Vanicat [11]. In a different direction, combinatorial and algebraic properties of two-species exclusion processes have been studied by Duchi and Schaeffer [12], Corteel, Mandelshtam and Williams [13], Mandelshtam and Viennot [14] and Cantini [15].

In this article, we focus on one of the integrable classes of two-species exclusion processes, where the slower particle can only enter and exit from the left boundary. We call this the *left-permeable two-species ASEP*. We begin with the preliminaries in Section 2. We derive the matrix product solution for the stationary distribution in Section 3 and find a representation of the matrix algebra in Section 4. We find the phase diagram of the model in the thermodynamic limit and derive formulas for the densities and current in all phases in Section 5. We end by computing the enriched phase diagrams for two different order parameters in Section 5.2: the density of the slower particle at the last site, and the difference of bulk and boundary densities for both species. We note that a large part of these calculations are generalisations of Uchiyama’s techniques [9].

## 2 Preliminaries

### 2.1 Definition of the model

The two-species ASEP describes particles hopping on a one dimensional lattice. We consider a finite lattice of length  $L$  where each lattice site is either empty, or occupied by a single particle of species 1 or 2. Particles move along the lattice by exchanging places with their immediate neighbours. We can consider an empty site as a particle of species 0, and then specify a lattice configuration by the tuple  $\boldsymbol{\tau} = (\tau_1, \dots, \tau_L)$ ,  $\tau_i \in \{0, 1, 2\}$ . In the bulk, exchanges between neighbouring particles occur with rates

$$\tau_i \tau_{i+1} \rightarrow \tau_{i+1} \tau_i \text{ with rate } \begin{cases} p, & \tau_i > \tau_{i+1}, \\ q, & \tau_i < \tau_{i+1}. \end{cases} \quad (2.1)$$

We will take  $p > q$  so that a particle of species  $j$  moves preferentially to the right ahead of all species  $i < j$ .

At the boundaries, we allow particles to enter and exit with the following rates:

- Left boundary:

$$\begin{aligned} 0 &\rightarrow 1 \text{ with rate } \gamma, \\ 0, 1 &\rightarrow 2 \text{ with rate } \alpha, \\ 2 &\rightarrow 1 \text{ with rate } \tilde{\gamma}. \end{aligned} \quad (2.2)$$

- Right boundary:



The rate  $\tilde{\gamma}$  is fixed as

$$\tilde{\gamma} = \frac{\alpha + \gamma + q - p}{\alpha + \gamma} \gamma. \tag{2.4}$$

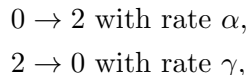
The other rates  $p, q, \alpha, \gamma, \beta, \delta$  can be arbitrary positive real numbers, subject to the constraint

$$\alpha + \gamma + q - p \geq 0, \tag{2.5}$$

so that  $\tilde{\gamma}$  is not negative. With this choice of rates, the model is integrable [10, 16]. Although we will not make direct use of the machinery of integrability, we will see that the constraint (2.4) also arises directly from the matrix product algebra approach.

The boundary rates (2.2), (2.3) allow species 2 to enter and exit at both boundaries. With  $q < p$  there will be a non-zero current of these particles from left to right, and so the system is out of equilibrium. In contrast, species 1 can only enter exit at the left boundary, and so although this species is driven in the bulk, its net current will be zero. Because species 1 is blocked by the right boundary but not by the left, we say that this model is *left-permeable*.

If instead of the left boundary rates (2.2), we take



(keeping the right-boundary rates (2.3)), species 1 is trapped on the lattice. We call this the semipermeable ASEP. Again, the net current of species 1 is zero, but in addition the *number* of particles of species 1 is fixed. Thus the system decomposes into sectors according to the number of particles of species 1 on the lattice. The stationary state for this model was found in matrix product form first for  $q = \gamma = \delta = 0$  [6] and then in general [9]. Later it was also studied through a Koornwinder polynomial approach [15]. In this work we will follow the approach of [9] and show that it can also be applied to the left-permeable model.

## 2.2 Markov process formulation

The models we have described are in fact continuous time Markov processes, which can be specified formally by giving the transition matrix. To do so, we must specify a basis. To a site  $i$ , with state given by  $\tau_i$ , we associate the standard basis vector  $|\tau_i\rangle \in \mathbb{C}^3$ , that is

$$|0\rangle = \begin{pmatrix} 1 \\ 0 \\ 0 \end{pmatrix}, \quad |1\rangle = \begin{pmatrix} 0 \\ 1 \\ 0 \end{pmatrix}, \quad |2\rangle = \begin{pmatrix} 0 \\ 0 \\ 1 \end{pmatrix}.$$

Then the lattice configuration is given by a vector  $|\boldsymbol{\tau}\rangle \in (\mathbb{C}^3)^{\otimes L}$ ,

$$|\boldsymbol{\tau}\rangle = |\tau_1, \dots, \tau_L\rangle = |\tau_1\rangle \otimes \dots \otimes |\tau_L\rangle.$$

The rates at which neighbouring particles exchange places (2.1) are encoded in the local transition matrix  $w \in \mathbb{C}^3 \otimes \mathbb{C}^3$ ,

$$w = \begin{pmatrix} 0 & 0 & 0 & 0 & 0 & 0 & 0 & 0 & 0 \\ 0 & -q & 0 & p & 0 & 0 & 0 & 0 & 0 \\ 0 & 0 & -q & 0 & 0 & 0 & p & 0 & 0 \\ 0 & q & 0 & -p & 0 & 0 & 0 & 0 & 0 \\ 0 & 0 & 0 & 0 & 0 & 0 & 0 & 0 & 0 \\ 0 & 0 & 0 & 0 & 0 & -q & 0 & p & 0 \\ 0 & 0 & q & 0 & 0 & 0 & -p & 0 & 0 \\ 0 & 0 & 0 & 0 & 0 & q & 0 & -p & 0 \\ 0 & 0 & 0 & 0 & 0 & 0 & 0 & 0 & 0 \end{pmatrix}, \quad (2.6)$$

acting on the ordered basis,

$$\{|0, 0\rangle, |0, 1\rangle, |0, 2\rangle, |1, 0\rangle, |1, 1\rangle, |1, 2\rangle, |2, 0\rangle, |2, 1\rangle, |2, 2\rangle\}.$$

The boundary rates (2.2), (2.3) are encoded (respectively) by matrices  $B, \bar{B} \in \mathbb{C}^3$ :

$$B = \begin{pmatrix} -\alpha - \gamma & 0 & 0 \\ \gamma & -\alpha & \tilde{\gamma} \\ \alpha & \alpha & -\tilde{\gamma} \end{pmatrix}, \quad \bar{B} = \begin{pmatrix} -\delta & 0 & \beta \\ 0 & 0 & 0 \\ \delta & 0 & -\beta \end{pmatrix}. \quad (2.7)$$

The complete transition matrix is then given by the sum of local matrices

$$M = B_1 + \sum_{i=1}^{L-1} w_{i,i+1} + \bar{B}_L. \quad (2.8)$$

The subscripts indicate the sites on which each matrix acts. That is,

$$B_1 = B \otimes I^{(L-1)}, \quad w_{i,i+1} = I^{(i-1)} \otimes w \otimes I^{(L-i-1)}, \quad \bar{B}_L = I^{(L-1)} \otimes \bar{B},$$

where  $I^{(k)}$  is the identity matrix on the  $k$ -fold tensor product of  $\mathbb{C}^3$ .

Writing  $P_\tau(t)$  for the probability of a configuration  $\tau$  at time  $t$ , the time evolution is determined by the master equation

$$\frac{d}{dt}|P(t)\rangle = M|P(t)\rangle, \quad \text{where } |P(t)\rangle = \sum_{\tau} P_\tau(t)|\tau\rangle.$$

At late times, the system converges to the stationary distribution of the process given by the normalised eigenvector of  $M$  with eigenvalue 0. That is, with

$$|\Psi\rangle = \sum_{\tau} \psi_\tau |\tau\rangle, \quad M|\Psi\rangle = 0,$$

the stationary distribution is

$$|P_{\text{stat}}\rangle = \frac{1}{Z_L} |\Psi\rangle, \quad Z_L = \sum_{\tau} \psi_\tau.$$

We will see later that the normalisation  $Z_L$  plays a role analogous to that of the partition function in equilibrium statistical mechanics. We will, with some abuse of terminology, refer to  $Z_L$  as the partition function throughout the paper.

From the stationary distribution we can compute the density of species  $k = 1, 2$  at site  $i$

$$\rho_i^{(k)} = \frac{1}{Z_L} \sum_{\tau_i=k} \psi_{\tau},$$

and we write  $\rho^{(k)}$  for the density averaged across the lattice. We can also compute the current  $J^{(2)}$ , of species 2: the probability per unit time that a particle of species 2 crosses a fixed point on the lattice (see (3.10)). Recall that the net current of species 1 is zero.

There is also a *right-permeable* two-species model analogous to the left-permeable model, with boundary matrices

$$B = \begin{pmatrix} -\alpha & 0 & \gamma \\ 0 & 0 & 0 \\ \alpha & 0 & -\gamma \end{pmatrix}, \quad \bar{B} = \begin{pmatrix} -\tilde{\delta} & \beta & \beta \\ \tilde{\delta} & -\beta & \delta \\ 0 & 0 & -\beta - \delta \end{pmatrix},$$

with

$$\tilde{\delta} = \frac{\beta + \delta + p - q}{\beta + \delta} \delta,$$

and the same bulk matrix (2.6). If we write the unnormalised stationary state vector for the left-permeable model as

$$|\Psi^{\text{left}}(\alpha, \beta, \gamma, \delta; p, q)\rangle = \sum_{\tau} \psi_{\tau}^{\text{left}}(\alpha, \beta, \gamma, \delta; p, q) |\tau\rangle,$$

the weights for the right-permeable model are given by

$$\psi_{\tau}^{\text{right}}(\alpha, \beta, \gamma, \delta; p, q) = \psi_{\tilde{\tau}}^{\text{left}}(\beta, \alpha, \delta, \gamma; q, p), \quad \tilde{\tau}_i = 2 - \tau_{L-i+1}.$$

Note for the right-permeable model, we take  $q > p$ . Taking  $q < p$  would correspond to a reverse-biased regime, where the boundary rates oppose the preferred direction of flow in the bulk [17, 18].

### 2.3 Stationary phase diagram of the semipermeable ASEP

We first review the key features of the stationary state of the semipermeable ASEP, since this will be useful for us later. The full phase diagram was computed in [9] using a matrix product algebra [1, 19]. The phase diagram has the same general structure as that of the single species ASEP [20, 21].

The key quantities of interest are the current and average density of the particles of species 2,  $J^{(2)}$  and  $\rho^{(2)}$ , respectively. As species 1 is trapped on the lattice, the average density  $\rho^{(1)}$  is a fixed parameter. The other parameters determining the phases of the system are expressed as the combinations of rates

$$a = \kappa_{\alpha, \gamma}^+, \quad c = \kappa_{\alpha, \gamma}^-, \quad b = \kappa_{\beta, \delta}^+, \quad d = \kappa_{\beta, \delta}^-, \quad (2.9)$$

where

$$\kappa_{u, v}^{\pm} = \frac{1}{2u} \left( p - q - u + v \pm \sqrt{(p - q - u + v)^2 + 4uv} \right).$$

This parameterisation satisfies  $a, b \geq 0$ , and with  $p > q$ ,  $-1 < c, d \leq 0$ .

The phase diagram, shown in Figure 1, depends only on  $a, b$ , and the density  $\rho^{(1)}$ . We name the phases according to the behaviour of species 2. The current and average density in these phases are:

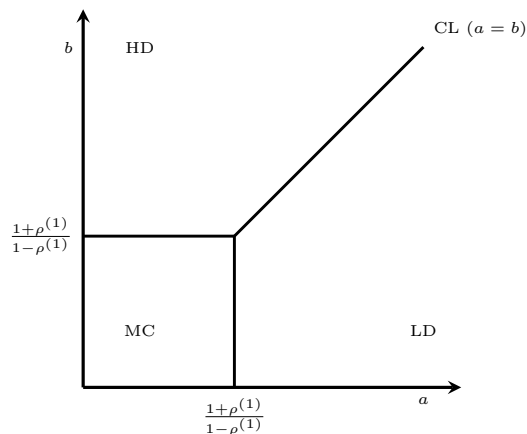


**Figure 1:** Stationary phase diagram of the semipermeable two-species ASEP. The density of species 1,  $\rho^{(1)}$  is a fixed parameter in this system.

- Maximum current (MC) phase:  $a, b < (1 + \rho^{(1)})/(1 - \rho^{(1)})$ , with

$$\rho^{(2)} = \frac{1 - \rho^{(1)}}{2}, \quad J^{(2)} = \frac{(p - q)(1 - \rho^{(1)2})}{4};$$

- Low density (LD) phase:  $a > (1 + \rho^{(1)})/(1 - \rho^{(1)})$ ,  $a > b$ , with

$$\rho^{(2)} = \frac{1}{1 + a}, \quad J^{(2)} = \frac{(p - q)a}{(1 + a)^2};$$

- High density (HD) phase:  $b > (1 + \rho^{(1)})/(1 - \rho^{(1)})$ ,  $b > a$ , with

$$\rho^{(2)} = \frac{b}{1 + b} - \rho^{(1)}, \quad J^{(2)} = \frac{(p - q)b}{(1 + b)^2}.$$

The line  $a = b > 1$  separating the high and low density phases is called the coexistence line (CL). Here both high and low density domains can exist on the lattice. This situation also exists for the single species ASEP, and is described by a domain wall model [22].

### 3 Stationary state for the left-permeable two-species ASEP

In this section we give a matrix product algebra and representation for the left-permeable two-species ASEP with boundary matrices (2.7). From this point on we fix the rightwards hopping rate to  $p = 1$ . We can do this without loss of generality, as it corresponds to rescaling the unit of time.

#### 3.1 Matrix product algebra

To write the stationary probabilities in matrix product form, define two vectors,

$$X = \begin{pmatrix} E \\ A \\ D \end{pmatrix}, \quad x = \begin{pmatrix} -1 \\ 0 \\ 1 \end{pmatrix}.$$

The entries of  $X$  ( $E, A, D$ ) are matrices in some auxiliary space. We take  $\langle\langle W|, |V\rangle\rangle$  as left and right vectors in this space that contract the matrices to give scalar values. We write the unnormalised stationary vector as

$$|\Psi\rangle = \langle\langle W|X \otimes \dots \otimes X|V\rangle\rangle, \quad (3.1)$$

so that

$$\psi_\tau = \langle\langle W|X_{\tau_1} \dots X_{\tau_L}|V\rangle\rangle.$$

That is to say, in every configuration, the occurrence of 0 is represented by  $E$ , 1 by  $A$ , and 2 by  $D$ . In order for this construction to give the stationary state, it is sufficient to find matrices  $E, A, D$  and vectors  $\langle\langle W|, |V\rangle\rangle$  for which the following conditions hold:

$$B\langle\langle W|X = \langle\langle W|x, \quad wX \otimes X = -x \otimes X + X \otimes x, \quad \bar{B}X|V\rangle\rangle = -x|V\rangle\rangle. \quad (3.2)$$

If we apply the transition matrix  $M$  of form (2.8) to  $|\Psi\rangle$  given by (3.1), these relations cause the bulk sum to telescope to two terms, which are cancelled by the left and right boundary terms (see [1, 19, 23] where this is discussed in more detail). It is important to note that we must also show that relations (3.2) are consistent. We will do this, in the usual manner, by giving explicit matrices  $E, D, A$ , and boundary vectors  $\langle\langle W|, |V\rangle\rangle$  that satisfy the relations (3.2). In fact, we will see that all we require is a representation of same algebra as used for the semipermeable model in [9], and we review that representation in Section 4.

With  $w$  given by (2.6), the bulk relations implied by (3.2) are

$$\begin{aligned} DE - qED &= D + E, \\ AE - qEA &= A, \\ DA - qAD &= A. \end{aligned} \quad (3.3)$$

And with boundary matrices (2.7), the boundary relations are

$$\begin{aligned} (\alpha + \gamma)\langle\langle W|E &= \langle\langle W|, \\ \gamma\langle\langle W|E - \alpha\langle\langle W|A + \tilde{\gamma}\langle\langle W|D &= 0, \\ -\delta E|V\rangle\rangle + \beta D|V\rangle\rangle &= |V\rangle\rangle. \end{aligned} \quad (3.4)$$

Using these relations, any expression of the form (3.1) can be reduced to a scalar multiple of  $\langle\langle W|V\rangle\rangle$ . For small system sizes, we can compute the stationary weights in this way. Checking that the computed vector is in fact the eigenvector of the transition matrix (2.8) with eigenvalue zero, we find that it is *necessary* that  $\tilde{\gamma}$  takes on its integrable value (2.4). We will show that this constraint on the parameters is also sufficient by giving an explicit representation of this algebra.

The bulk relations (3.3) are the same as those from [9] for the semipermeable ASEP. Following [9], we express the bulk relations in terms of matrices  $\mathbf{e}, \mathbf{d}$ , satisfying the  $q$ -deformed oscillator algebra [20],

$$\mathbf{d}\mathbf{e} - q\mathbf{e}\mathbf{d} = 1 - q. \quad (3.5)$$

Then

$$\begin{aligned} D &= \frac{1}{1-q}(1 + \mathbf{d}), & E &= \frac{1}{1-q}(1 + \mathbf{e}), \\ A &= \lambda(DE - ED) = \frac{\lambda}{1-q}(1 - \mathbf{e}\mathbf{d}), \end{aligned}$$

satisfy the bulk algebra, with  $\lambda$  a free parameter. We will write the boundary relations as

$$\begin{aligned} \langle\langle W|\mathbf{e} + ac\langle\langle W|\mathbf{d} = (a + c)\langle\langle W|, \\ \mathbf{d}|V\rangle\rangle + bde|V\rangle\rangle = (b + d)|V\rangle\rangle. \end{aligned} \quad (3.6)$$

This is the form used for the semipermeable ASEP [9], and also the single species ASEP [21]. In both these case the parameters  $a, b, c, d$  are those appearing in the stationary state of the ASEP (see (2.9)).

The boundary relations (3.4) for the left-permeable two-species ASEP can also be written in the form (3.6), but now we take

$$\lambda = \frac{\gamma}{\alpha}, \quad a = 0, \quad c = \frac{1 - q - \alpha - \gamma}{\alpha + \gamma}, \quad b = \kappa_{\beta, \delta}^+, \quad d = \kappa_{\beta, \delta}^-, \quad (3.7)$$

and require also that  $\tilde{\gamma}$  takes its value given in (2.4). With the constraint (2.5), we can write

$$a = \kappa_{\alpha + \gamma, 0}^+, \quad c = \kappa_{\alpha + \gamma, 0}^-$$

and

$$-1 < c \leq 0, \quad (3.8)$$

where the lower bound assumes that  $q < 1$ .

Representations of the algebra (3.5), (3.6) are well known, and in Section 4.2 we will give the explicit form of the representation used in [9]. As we know a representation exists, the matrix product relations for the left-permeable two-species ASEP are consistent, and can be used to calculate the stationary state. But first, we describe the main physical quantities of interest, and how they are calculated.

### 3.2 Physical quantities

The stationary probabilities are obtained by normalising the stationary weights (3.1). Thus

$$P_{\tau} = \frac{1}{Z_L} \langle\langle W|X_{\tau_1} \dots X_{\tau_L}|V\rangle\rangle, \quad (3.9)$$

with

$$Z_L = \langle\langle W|C^L|V\rangle\rangle, \quad C = E + D + A.$$

The current of type 2 particles is given by

$$J^{(2)} = \frac{1}{Z_L} \langle\langle W|C^{i-1} (DE - qED + DA - qAD) C^{L-i-1}|V\rangle\rangle = \frac{Z_{L-1}}{Z_L}, \quad (3.10)$$

which is independent of position,  $i$ . The net current of type 1 particles must be zero as they can only enter at the left boundary. Indeed, computing with the matrix product algebra, we find

$$J^{(1)} = \frac{1}{Z_L} \langle\langle W|C^{i-1} (AE - qEA + qAD - DA) C^{L-i-1}|V\rangle\rangle = 0.$$

We would also like to compute the average density of species  $k = 1, 2$ , which is given by

$$\rho^{(k)} = \frac{1}{L} \frac{1}{Z_L} \sum_{i=1}^L \langle\langle W|C^{i-1} X_k C^{L-i}|V\rangle\rangle. \quad (3.11)$$



To achieve this, we define

$$Z_L(\xi^2, \zeta) = \langle\langle W | (E + \xi^2 D + \zeta A)^L | V \rangle\rangle, \quad (3.12)$$

which plays the role of a partition function with fugacities  $\xi^2, \zeta$  for type 1 and 2 particles respectively. Then

$$\begin{aligned} \rho^{(1)} &= \frac{1}{L} \frac{\partial}{\partial \zeta} \log Z_L(\xi^2, \zeta) \Big|_{\xi^2=\zeta=1}, \\ \rho^{(2)} &= \frac{1}{L} \frac{\partial}{\partial \xi^2} \log Z_L(\xi^2, \zeta) \Big|_{\xi^2=\zeta=1}. \end{aligned} \quad (3.13)$$

In order to compute the partition function defined in (3.12), it will be convenient to rewrite it as

$$Z_L(\xi^2, \zeta) = \left( \frac{\xi}{1-q} \right)^L \langle\langle W | (\xi^{-1} + \xi + \bar{\mathbf{e}} + \bar{\mathbf{d}} + (1-q)\bar{\zeta}A)^L | V \rangle\rangle, \quad (3.14)$$

with

$$\bar{\mathbf{e}} = \xi^{-1} \mathbf{e}, \quad \bar{\mathbf{d}} = \xi \mathbf{d}, \quad \bar{\zeta} = \zeta \xi^{-1}.$$

The rescaled generators  $\bar{\mathbf{e}}, \bar{\mathbf{d}}$  satisfy the same  $q$ -oscillator algebra (3.5). Defining also

$$\bar{a} = \xi^{-1} a, \quad \bar{c} = \xi^{-1} c, \quad \bar{b} = \xi b, \quad \bar{d} = \xi d,$$

the boundary relations for the rescaled generators are obtained by putting bars over the boundary parameters  $a, b, c, d$  in (3.6). Thus, given a representation of the original algebra, we obtain a representation of the scaled algebra, simply by replacing the boundary parameters by their barred versions.

## 4 Representation of the algebra and the partition function

For the representation of the algebra we use exactly that from [9], but with parameters specialised differently. We then review how this is used to find an integral form for the partition function.

### 4.1 Continuous big $q$ -Hermite polynomials

To give the representation of the algebra, we must first introduce certain notation from the ‘ $q$ -calculus’ [24, 25]. The  $q$ -shifted factorial is given by

$$(a_1, \dots, a_s; q)_n = \prod_{r=1}^s (a_r; q)_n,$$

where

$$(a; q)_n = \prod_{k=0}^{n-1} (1 - aq^k) = (1-a)(1-aq) \cdots (1-aq^{n-1}),$$

valid also for  $n \rightarrow \infty$  when  $q < 1$ . The basic hypergeometric series is given by

$${}_r\phi_s \left[ \begin{matrix} a_1, \dots, a_r \\ b_1, \dots, b_s \end{matrix} \middle| q, z \right] = \sum_{k=0}^{\infty} \frac{(a_1, \dots, a_r; q)_k}{(q, b_1, \dots, b_s; q)_k} \left( (-1)^k q^{\binom{k}{2}} \right)^{1+s-r} z^k.$$

Following [9], we define

$$F_n(u, v; \lambda) = \sum_{k=0}^n \frac{(q; q)_n}{(q; q)_k (q; q)_{n-k}} (\lambda u; q)_k v^k u^{n-k},$$

which satisfies the recurrence relation

$$F_{n+1}(u, v; \lambda) + \lambda uv q^n F_n(u, v; \lambda) + (1 - q^n) uv F_{n-1}(u, v; \lambda) = (u + v) F_n(u, v; \lambda),$$

with  $F_{-1} = 0$  and  $F_0 = 1$ . Specialisation of the parameters  $u, v$  gives the *continuous big  $q$ -Hermite polynomial* [25],

$$H_n(\cos \theta; \lambda | q) = F_n(e^{i\theta}, e^{-i\theta}; \lambda).$$

For  $\lambda$  real and  $|\lambda| < 1$ ,  $H_n(\cos \theta; \lambda | q)$  satisfies the orthogonality relation

$$\int_0^\pi \frac{d\theta}{2\pi} w(\cos \theta; \lambda) H_m(\cos \theta; \lambda | q) H_n(\cos \theta; \lambda | q) = (q; q)_n \delta_{mn}, \quad (4.1)$$

with

$$w(\cos \theta; \lambda) = w(e^{i\theta}, e^{-i\theta}; \lambda) = \frac{(q, e^{2i\theta}, e^{-2i\theta}; q)_\infty}{(\lambda e^{i\theta}, \lambda e^{-i\theta}; q)_\infty}. \quad (4.2)$$

Alternatively, we can write (4.1) as the contour integral

$$\oint \frac{dz}{4\pi iz} w(z, z^{-1}; \lambda) H_m\left(\frac{z + z^{-1}}{2}; \lambda | q\right) H_n\left(\frac{z + z^{-1}}{2}; \lambda | q\right) = (q; q)_n \delta_{mn}, \quad (4.3)$$

where the contour of integration is the unit circle. The orthogonality condition for  $\lambda > 1$  is obtained from (4.3) by deforming the contour of integration: such that the origin and all poles at  $\lambda q^k$  are included, and all poles at  $\lambda^{-1} q^{-k}$  are excluded, with  $k = 0, 1, 2, \dots$

We will need the  $q$ -Mehler-type sum formula given in [9] (see also [26]) for  $|\tau u|, |\tau v| < 1$ :

$$\sum_{n=0}^{\infty} \frac{\tau^n}{(q; q)_n} H_n(\cos \theta; \lambda | q) F_n(u, v; 0) = \Theta(\cos \theta; \tau u, \tau v | \lambda) \quad (4.4)$$

with

$$\begin{aligned} \Theta(\cos \theta; u, v | \lambda) &= \Theta(e^{i\theta}, e^{-i\theta}; u, v | \lambda) \\ &= \frac{(\lambda u, \lambda v; q)_\infty}{(u e^{i\theta}, u e^{-i\theta}, v e^{i\theta}, v e^{-i\theta}; q)_\infty} {}_2\phi_2 \left[ \begin{matrix} \lambda e^{i\theta}, \lambda e^{-i\theta} \\ \lambda u, \lambda v \end{matrix} \middle| q, uv \right]. \end{aligned} \quad (4.5)$$

For the model we consider, we will need to take  $u = 0$  (or equivalently  $v = 0$ ), and can do this by taking the limit  $u \rightarrow 0$ . For convenience, we will write

$$\begin{aligned} F_n(0, v; \lambda) &= \lim_{u \rightarrow 0} F_n(u, v; \lambda) = v^n, \quad \text{and} \\ {}_2\phi_2 \left[ \begin{matrix} \lambda e^{i\theta}, \lambda e^{-i\theta} \\ 0, \lambda v \end{matrix} \middle| q, 0 \right] &= \lim_{u \rightarrow 0} {}_2\phi_2 \left[ \begin{matrix} \lambda e^{i\theta}, \lambda e^{-i\theta} \\ \lambda u, \lambda v \end{matrix} \middle| q, uv \right] = 1. \end{aligned}$$

Note also that if  $|\tau u| > 1$  or  $|\tau v| > 1$ , the sum in (4.4) is divergent as, for example, if  $|u| > |v|$ ,  $F_n(u, v; 0) \sim u^n$  for large  $n$ .

## 4.2 Representation

The  $q$ -oscillator algebra (3.5) has a Fock space representation

$$\mathbf{d} = \sum_{n=1}^{\infty} \sqrt{1-q^n} |n-1\rangle\langle n|, \quad \mathbf{e} = \sum_{n=0}^{\infty} \sqrt{1-q^{n+1}} |n+1\rangle\langle n|, \quad (4.6)$$

and therefore

$$A = \frac{\lambda}{1-q} \sum_{n=0}^{\infty} q^n |n\rangle\langle n|.$$

Writing the boundary vectors as

$$\langle\langle W| = \sum_{n=0}^{\infty} w_n \langle n|, \quad |V\rangle\rangle = \sum_{n=0}^{\infty} v_n |n\rangle, \quad (4.7)$$

then from the boundary relations (3.6), the coefficients must satisfy

$$\begin{aligned} \sqrt{(q;q)_{n+1}} w_{n+1} - (a+c) \sqrt{(q;q)_n} w_n + ac(1-q^n) \sqrt{(q;q)_{n-1}} w_{n-1} &= 0, \\ \sqrt{(q;q)_{n+1}} v_{n+1} - (b+d) \sqrt{(q;q)_n} v_n + bd(1-q^n) \sqrt{(q;q)_{n-1}} v_{n-1} &= 0. \end{aligned}$$

These recurrences are solved by taking

$$w_n = \frac{F_n(a, c; 0)}{\sqrt{(q;q)_n}}, \quad v_n = \frac{F_n(b, d; 0)}{\sqrt{(q;q)_n}}. \quad (4.8)$$

Note that as we have  $a = 0$ ,  $w_n$  has the simpler form

$$w_n = \frac{c^n}{\sqrt{(q;q)_n}}.$$

With (4.6), (4.7), (4.8), we have a representation of the algebra (3.5), (3.6).

In order to compute the partition function  $Z(\xi^2, \zeta)$ , we start from the form (3.14). The trick is to find a solution of the eigenvalue equation

$$(\bar{\mathbf{e}} + \bar{\mathbf{d}} + (1-q)\bar{\zeta}A)|h(\cos\theta)\rangle\rangle = 2\cos\theta|h(\cos\theta)\rangle\rangle. \quad (4.9)$$

Using the representation (4.6) (which also gives a representation of the barred algebra), we find

$$|h(\cos\theta)\rangle\rangle = \sum_{n=0}^{\infty} \frac{H_n(\cos\theta; \lambda\zeta\xi^{-1}|q)}{\sqrt{(q;q)_n}} |n\rangle.$$

As  $(\bar{\mathbf{e}} + \bar{\mathbf{d}} + (1-q)\bar{\zeta}A)$  is a symmetric matrix, it has the transpose  $\langle\langle h\cos\theta|$  as a right eigenvector with the same eigenvalue. From the orthogonality condition (4.1), we then obtain

$$1 = \int_0^\pi \frac{d\theta}{2\pi} w(\cos\theta; \lambda\zeta\xi^{-1}) |h(\cos\theta)\rangle\rangle \langle\langle h(\cos\theta)|, \quad (4.10)$$

for  $|\lambda\zeta\xi^{-1}| < 1$ . For the case  $|\lambda\zeta\xi^{-1}| > 1$ , we use the contour integral form of the orthogonality condition, with the contour deformed as described below (4.3).

### 4.3 Partition function

Following [9, 21], we write the partition function in integral form. Starting from the partition function as given in (3.14), use (4.10) to insert the identity, then the eigenvalue equation (4.9), then finally the sum formula (4.4). This gives the integral form

$$\begin{aligned}
Z_L(\xi^2, \zeta) &= \int_0^\pi \frac{d\theta}{2\pi} w(\cos \theta; \lambda \zeta \xi^{-1}) \\
&\quad \times \Theta(\cos \theta; 0, \xi^{-1}c | \lambda \zeta \xi^{-1}) \Theta(\cos \theta; \xi b, \xi d | \lambda \zeta \xi^{-1}) \\
&\quad \times \left( \frac{1 + \xi^2 + 2\xi \cos \theta}{1 - q} \right)^L.
\end{aligned} \tag{4.11}$$

We have used the boundary vectors of the ‘barred’ algebra to obtain this expression. The form (4.11) is valid for  $|\zeta \xi^{-1} \lambda|, |\xi b|, |\xi^{-1} c|, |\xi d| < 1$ . Recall also that for the left-permeable model we have  $a = 0$ .

In fact, in our model  $|c|, |d| < 1$ , and we can take  $\zeta, \xi$  arbitrarily close to 1. Thus we need only be concerned with the cases where  $\lambda > 1$  or  $b > 1$ . For these cases, we write the partition function in (4.11) by changing to the variable  $z = e^{i\theta}$  as

$$\begin{aligned}
Z_L(\xi^2, \zeta) &= \oint \frac{dz}{4\pi i z} w(z, z^{-1}; \lambda \zeta \xi^{-1}) \\
&\quad \times \Theta(z, z^{-1}; 0, \xi^{-1}c | \lambda \zeta \xi^{-1}) \Theta(z, z^{-1}; \xi b, \xi d | \lambda \zeta \xi^{-1}) \\
&\quad \times \left( \frac{(1 + \xi z)(1 + \xi z^{-1})}{1 - q} \right)^L,
\end{aligned} \tag{4.12}$$

where for the contour of integration we take the unit circle deformed to include all poles at  $z = \lambda \zeta \xi^{-1} q^k, z = \xi b q^k$ , and exclude all poles at  $z = 1/(\lambda \zeta \xi^{-1} q^k), z = 1/(\xi b q^k)$ , with  $k = 0, 1, 2, \dots$

The deformation to include/exclude the  $\lambda$  poles follows from the orthogonality condition (4.3). The case with  $b > 1$  is less straightforward. With  $b > 1$ , the product  $\langle\langle h(\cos \theta) | V \rangle\rangle$ , which appears when we compute the partition function, is in fact a divergent sum. A representation without this problem is known for the single species ASEP [21], but not in the multispecies case. However, the deformation of the contour for the  $b > 1$  case can be justified as the analytic continuation of the partition function [1, 17].

## 5 Stationary properties in the thermodynamic limit

For finite sizes, the integral form of the partition function  $Z_L(\xi^2, \zeta)$  is difficult to work with. However, it is possible to extract its asymptotic behaviour when  $L$  is large, allowing the computation of stationary currents and densities.

### 5.1 Phase diagram

To find the phase diagram of the model, we need to find an asymptotic form of the partition function. And the key to the asymptotics of the partition function are the poles due to  $\lambda, b$  in the integral form. For  $\lambda, b < 1$ , the asymptotic form can be obtained from the form (4.11) following the method in [27], or by a saddle-point analysis of the complex integral (4.12) [17]. For  $\lambda > 1$  (or similarly  $b > 1$ ) we must subtract the

contribution of the poles at  $z = 1/(\lambda\zeta\xi^{-1}q^k)$  from this result, and add the contribution of the poles at  $z = \lambda\zeta\xi^{-1}q^k$  (see [19] for a detailed explanation). The contribution from the poles with  $k = 0$  give the dominant asymptotic behaviour.

From the asymptotic form of the partition function we can compute the species 2 current through (3.10), and the averaged densities of species 1 and 2 through (3.13). We find three phases, as in the model with semipermeable boundaries (see Figure 1), which we name according to the behaviour of the species 2.

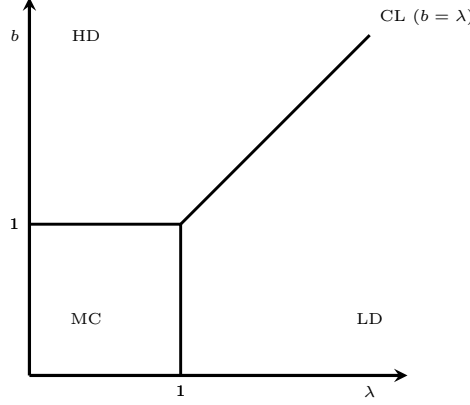


**Figure 2:** Phase diagram for lattice average current and density with  $\lambda = \gamma/\alpha$ .

- Maximum current phase (MC): For  $\lambda < 1$  and  $b < 1$ , the asymptotic form of the partition function is

$$Z_L(\xi^2, \zeta) \simeq \frac{(q; q)_\infty^3 (\zeta\lambda b, \zeta\xi^{-2}\lambda c, \zeta\lambda d; q)_\infty}{(\zeta\xi^{-1}\lambda, \xi b, \xi^{-1}c, \xi d; q)_\infty^2} {}_2\phi_2 \left[ \begin{matrix} \zeta\xi^{-1}\lambda, \zeta\xi^{-1}\lambda \\ \zeta\lambda b, \zeta\lambda d \end{matrix} \middle| q, \xi^2 bd \right] \\ \times \frac{[(1+\xi)(1+\xi^{-1})]^{3/2}}{2\sqrt{\pi}L^{3/2}} \left[ \frac{(1+\xi)^2}{1-q} \right]^L.$$

From this we obtain the currents and average densities

$$J^{(2)} = \frac{1-q}{4}, \quad \rho^{(1)} = \mathcal{O}(1/L), \quad \rho^{(2)} = \frac{1}{2}.$$

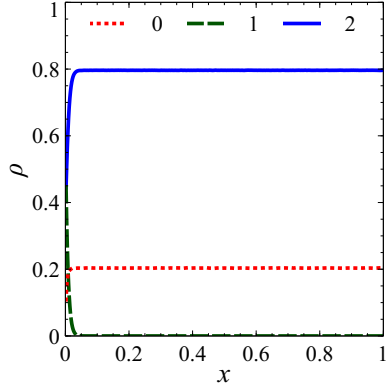
The complete leading order term of the density  $\rho^{(1)}$  can be computed through (3.13), but we have not found a simple expression for it.

- Low density phase (LD): For  $\lambda > 1$ ,  $\lambda > b$ , the leading term comes from adding (subtracting) the contribution of the pole at  $z = \zeta\xi^{-1}\lambda$  ( $z = 1/(\zeta\xi^{-1}\lambda)$ ), and gives

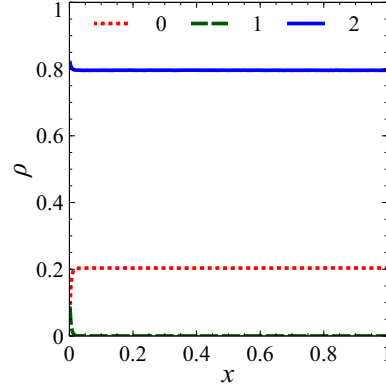
$$Z_L(\xi^2, \zeta) \simeq \frac{(\zeta^{-2}\xi^2\lambda^{-2}; q)_\infty}{(\zeta^{-1}\xi^2b/\lambda, \zeta^{-1}c/\lambda, \zeta^{-1}\xi^2d/\lambda; q)_\infty} \left( \frac{(1+\zeta\lambda)(1+\zeta^{-1}\xi^2\lambda^{-1})}{1-q} \right)^L.$$

From this we obtain

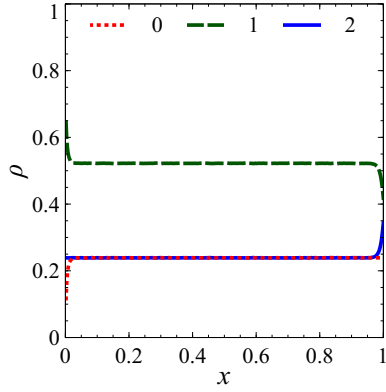
$$J^{(2)} = \frac{(1-q)\lambda}{(1+\lambda)^2}, \quad \rho^{(1)} = \frac{\lambda-1}{1+\lambda}, \quad \rho^{(2)} = \frac{1}{1+\lambda}.$$



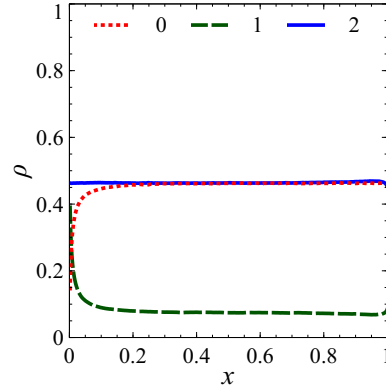
(a) Sub-phase HD1 for  $\lambda = 1.75, b = 3.91$ , and  $d = -0.66$  ( $\alpha = 0.32, \gamma = 0.56, \beta = 0.35, \delta = 0.9, q = 0.41$ ).



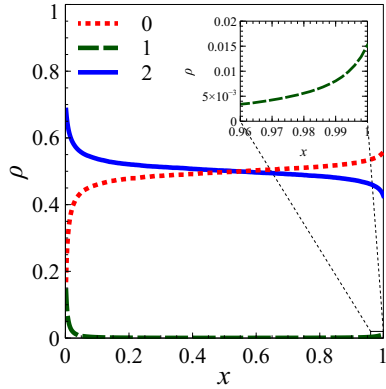
(b) Sub-phase HD2 for  $\lambda = 0.20, b = 3.91$ , and  $d = -0.66$  ( $\alpha = 0.81, \gamma = 0.16, \beta = .35, \delta = 0.9, q = 0.41$ ).



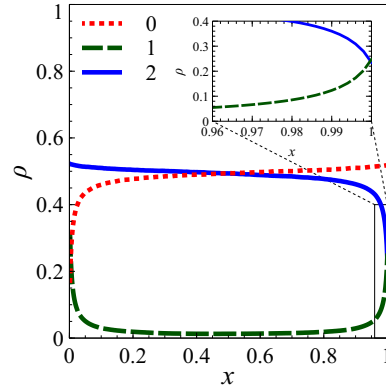
(c) Sub-phase LD1 for  $\lambda = 3.18, b = 1.25$ , and  $d = -0.59$  ( $\alpha = 0.22, \gamma = 0.7, \beta = 0.64, \delta = 0.47, q = 0.41$ ).



(d) Sub-phase LD2 for  $\lambda = 1.16, b = 0.94$ , and  $d = -0.68$  ( $\alpha = 0.5, \gamma = 0.58, \beta = 0.95, \delta = 0.61, q = 0.41$ ).



(e) MC phase for for  $\lambda = 0.37, b = 0.75, d = -0.59$  ( $\alpha = 0.62, \gamma = 0.23, \beta = 0.83, \delta = 0.37, q = 0.41$ ).



(f) MC phase for for  $\lambda = 0.91, b = 0.26$ , and  $d = -0.45$  ( $\alpha = 0.45, \gamma = 0.41, \beta = 0.85, \delta = 0.1, q = 0.41$ ).

**Figure 3:** Density profiles in the LD, HD and MC phases. Each plot shows densities of species 0 (red dotted line), 1 (green dashed line) and 2 (blue solid line) versus normalised site position  $x = i/L$  for  $L = 500$ . The sub-phases LD1, LD2, HD1 and HD2 will be described in Section 5.2.

- High density phase (HD): For  $b > 1$ ,  $b > \lambda$ , the leading term comes from adding (subtracting) the contribution of the pole at  $z = \xi b$  ( $z = 1/(\xi b)$ ), and gives

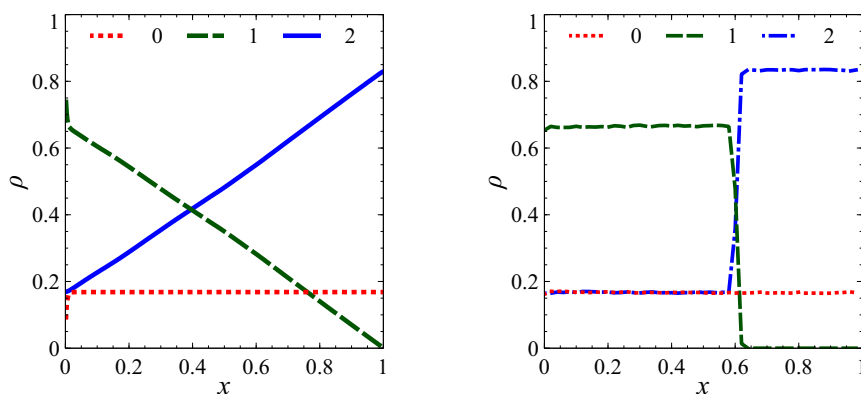
$$Z_L(\xi^2, \zeta) \simeq \frac{(\zeta \xi^{-2} \lambda c, \zeta \lambda d, \xi^{-2} b^{-2}; q)_\infty}{(\zeta \xi^{-2} \lambda / b, bc, \xi^{-2} c / b, \xi^2 b d, d / b; q)_\infty} {}_1\phi_1 \left[ \begin{matrix} \zeta \xi^{-2} \lambda / b \\ \zeta \lambda d \end{matrix} \middle| q, \xi^2 b d \right] \times \left( \frac{(1 + \xi^2 b)(1 + b^{-1})}{1 - q} \right)^L.$$

From this we obtain

$$J^{(2)} = \frac{(1 - q)b}{(1 + b)^2}, \quad \rho^{(1)} = \mathcal{O}(1/L), \quad \rho^{(2)} = \frac{b}{1 + b}.$$

Again, we have not found a simple expression for the density  $\rho^{(1)}$ .

The phase diagram is shown in Figure 2. Simulation results showing typical density profiles for each of the phases are shown in Figure 3. The sub-phases identified in those figures will be discussed in Section 5.2.



(a) Time-averaged densities for  $L = 500$ .

(b) Instantaneous density profiles for  $L = 2500$ , coarse-grained over 50 sites.

**Figure 4:** Time-averaged and instantaneous density profiles on the coexistence line for  $\lambda = 0.37$ ,  $b = 0.75$ ,  $d = -0.59$  ( $\alpha = 0.15$ ,  $\gamma = 0.74$ ,  $\beta = 0.28$ ,  $\delta = 0.89$ ,  $q = 0.41$ ). Each plot shows densities of species 0 (red dotted line), 1 (green dashed line) and 2 (blue solid line) versus normalised site position  $x = i/L$ .

As in the ASEP, there is a first order phase transition along the coexistence line (CL): that is, the line  $\lambda = b > 1$  separating the high and low density phases. On this line, high and low density domains coexist on the lattice. The left boundary attempts to impose a region characteristic of the low density phase, while the right boundary attempts to impose a region as in the high density phase. These two domains are separated by a moving shock, or domain wall [22]. The linear profiles shown in Figure 4(a) are characteristic of this situation when the position of the shock is averaged across the lattice. In Figure 4(b), we show an instantaneous density profile in this phase, with the shock captured at around  $0.6L$ . Figure 4(b) was obtained by taking a very large lattice length ( $L = 2500$ ), then computing a coarse-grained spatial density by averaging over windows of 50 sites.

## 5.2 Boundary densities

The simulation results show that the per-site density differs from the value averaged across the lattice. We can get some indication of this behaviour by computing the site densities

$$\rho_i^{(k)} = \frac{1}{Z_L} \langle\langle W | C^{i-1} X_k C^{L-i} | V \rangle\rangle, \quad (5.1)$$

for species  $k = 1, 2$  at the first and last sites. We can use the boundary algebra relations (3.4) to express the density at site 1 in terms of the current  $J^{(2)}$  (3.10). We obtain

$$\begin{aligned} \rho_1^{(1)} &= \frac{-c\lambda(1-q) + \lambda(1+c)^2 J^{(2)}}{(1-q)(1-c\lambda)}, \\ \rho_1^{(2)} &= \frac{1-q - (1+\lambda)(1+c)J^{(2)}}{(1-q)(1-c\lambda)}. \end{aligned} \quad (5.2)$$

Taking the value of  $J^{(2)}$  for each phase gives the density at the left boundary (see Table 1). At the right boundary we find

$$\rho_L^{(2)} = \frac{(1+b)(1+d)J^{(2)} - (1-q)bd}{(1-q)(1-bd)} + \frac{bd}{1-bd} \rho_L^{(1)}, \quad (5.3)$$

but the algebraic relations alone are not enough to give  $\rho_L^{(1)}$ . Instead we must return to the representation of the algebra. Again, we will use the trick of inserting the identity operator (4.10), but now we take  $\zeta = \xi = 1$ , and write

$$\begin{aligned} I_{L,k} &= \langle\langle W | C^{L-k} A^k | V \rangle\rangle \\ &= \int_0^\pi \frac{d\theta}{2\pi} w(\cos \theta; \lambda) \langle\langle W | C^{L-k} | h(\cos \theta) \rangle\rangle \langle\langle h(\cos \theta) | A^k | V \rangle\rangle, \end{aligned}$$

which will allow us to compute the probability that the  $k$  rightmost sites are occupied by particles of species 1. Using the representation of algebra, and the sum formula (4.4),

$$\begin{aligned} \langle\langle h(\cos \theta) | A^k | V \rangle\rangle &= \frac{\lambda^k}{(1-q)^k} \sum_{n=0}^{\infty} \frac{q^{kn}}{(q; q)_n} H_n(\cos \theta; \lambda|q) F_n(b, d; 0) \\ &= \Theta(\cos \theta; q^k b, q^k d | \lambda). \end{aligned}$$

Thus we find that the integral expression for  $I_{L,k}$  is (up to an overall factor) simply that of the partition function at length  $L - k$  with  $b \rightarrow q^k b$ ,  $d \rightarrow q^k d$ . That is,

$$I_{L,k} = \frac{\lambda^k}{(1-q)^k} Z_{L-k} \Bigg|_{\substack{b \rightarrow q^k b \\ d \rightarrow q^k d}},$$

where  $Z_L = Z_L(\xi^2 = 1, \zeta = 1)$ .

The asymptotic behaviour of  $I_{L,k}$  is the same as that for the partition function, except that the phase boundaries now depend on  $q^k b$  instead of on  $b$ . We will write  $Z_L^{\text{LD}}$ ,  $Z_L^{\text{HD}}$ ,  $Z_L^{\text{MC}}$ , to indicate the expression for the partition function in the low density, high density, or maximum current phases respectively. Then we write  $I_{L,k}^{\text{XX}}$  for the corresponding value of  $I_{L,k}$ , but with the phase boundaries determined by  $q^k b$ .



Now, the probability of having the  $k$  rightmost sites occupied by particles of type 1 is

$$P_{\text{jam}}^{(1)}(k) = P(\tau_{L-k+1} = \dots = \tau_L = 1) = \frac{I_{L,k}^{\text{YY}}}{Z_L^{\text{XX}}}. \quad (5.4)$$

Here XX, YY indicates the appropriate phase for each part of the expression: the XX phase boundaries are determined by  $(\lambda, b)$ , and the YY boundaries are determined by  $(\lambda, q^k b)$ . The density  $\rho_L^{(1)}$  is given by (5.4) with  $k = 1$ . We compute  $\rho_L^{(1)}$  for each possible phase combination, indicating these by the shorthand XX(YY):

- MC(MC) phase:  $\lambda, b < 1$ :

$$\rho_L^{(1)} = \frac{\lambda (1-b)^2 (1-d)^2}{4 (1-\lambda b)(1-\lambda d)} \left( \frac{L}{L-1} \right)^{3/2} \frac{{}_2\phi_2 \left[ \begin{matrix} \lambda, \lambda \\ q\lambda b, q\lambda d \end{matrix} \middle| q, q^2 bd \right]}{{}_2\phi_2 \left[ \begin{matrix} \lambda, \lambda \\ \lambda b, \lambda d \end{matrix} \middle| q, bd \right]}. \quad (5.5)$$

Note that  $\rho_L^{(1)}$  approaches a constant value for large  $L$ . Note also that for  $q, |bd| \ll 1$ , the  ${}_2\phi_2$  series in this expression are close to 1, and we can approximate

$$\rho_L^{(1)} \simeq \frac{\lambda (1-b)^2 (1-d)^2}{4 (1-\lambda b)(1-\lambda d)}.$$

- HD(MC) phase:  $\lambda < 1, 1 < b < q^{-1}$ :

$$\rho_L^{(1)} \sim \frac{1}{(L-1)^{3/2}} \left( \frac{4}{(1+b)(1+b^{-1})} \right)^L. \quad (5.6)$$

By ‘ $\sim$ ’ we mean the scaling behaviour with  $L$ . We do not write out the full expression, only because we have not found a simple form for it.

- HD(HD) phase:  $b > q^{-1}, b > q^{-1}\lambda$ :

$$\rho_L^{(1)} \sim \left( \frac{(1+qb)(1+q^{-1}b^{-1})}{(1+b)(1+b^{-1})} \right)^L. \quad (5.7)$$

- HD(LD) phase:  $\lambda > 1, \lambda < b < q^{-1}\lambda$ :

$$\rho_L^{(1)} \sim \left( \frac{(1+\lambda)(1+\lambda^{-1})}{(1+b)(1+b^{-1})} \right)^L. \quad (5.8)$$

- LD(LD) phase:  $\lambda > 1, \lambda > b$ :

$$\rho_L^{(1)} = \frac{(\lambda-b)(\lambda-d)}{(1+\lambda)^2}. \quad (5.9)$$

Taking  $\rho_L^{(1)}$  as the order parameter, the high density phase splits into sub-phases according to the scaling behaviour. However across all these high density sub-phases, the density  $\rho_L^{(1)}$  scales as  $z^L$  or  $z^L/L^{3/2}$  with  $z < 1$ . These sub-phases are depicted in Figure 5

The maximum current and low density phases do not split into sub-phases, and the leading order behaviour is constant in  $L$ . The expressions for  $P_{\text{jam}}^{(1)}(k)$  in these phases are non-vanishing (with  $L$ ):

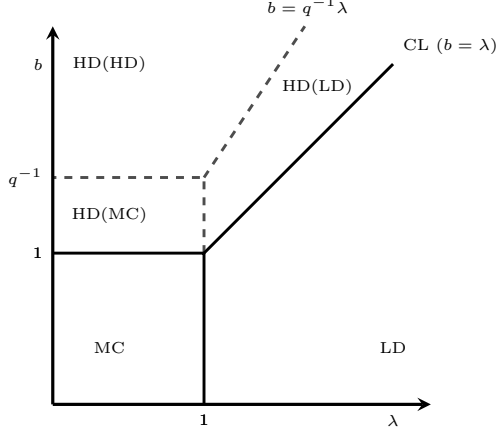


**Figure 5:** Division of the HD phase according to the scaling of  $\rho_L^{(1)}$ , as given in (5.6) – (5.8).

- MC(MC) phase:  $\lambda, b < 1$ :

$$P_{\text{jam}}^{(1)}(k) = \left(\frac{\lambda}{4}\right)^k \frac{(b, d; q)_k^2}{(\lambda b, \lambda d; q)_k} \left(\frac{L}{L-k}\right)^{3/2} {}_{2\phi_2} \left[ \begin{matrix} \lambda, \lambda \\ q^k \lambda b, q^k \lambda d \end{matrix} \middle| q, q^{2k} b d \right] / {}_{2\phi_2} \left[ \begin{matrix} \lambda, \lambda \\ \lambda b, \lambda d \end{matrix} \middle| q, b d \right].$$

- LD(LD) phase:  $\lambda > 1, \lambda > b$ :

$$P_{\text{jam}}^{(1)}(k) = \frac{\lambda^k (\lambda^{-1} b, \lambda^{-1} d; q)_k}{(1 + \lambda)^{2k}}.$$

It is perhaps surprising to find that in the MC phase, species 1 has a fixed finite density at the right boundary for large  $L$ , even as the bulk density vanishes as  $1/L$  (see (5.5)). The insets in Figures 3(e), 3(f) show close-ups of such density profiles. The simulation results and analytically calculated values are in good agreement.

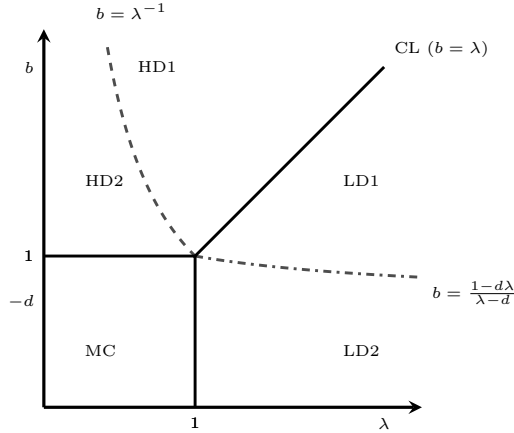
Phase	$\rho_1^{(1)} - \rho^{(1)}$	$\rho_1^{(2)} - \rho^{(2)}$	$\rho_L^{(1)} - \rho^{(1)}$	$\rho_L^{(2)} - \rho^{(2)}$
MC ( $\lambda, b < 1$ )	$\frac{(1-c)^2}{4(1-c\lambda)}$	$\frac{(1-c)(1-\lambda)}{4(1-c\lambda)}$	$\rho_L^{(1)}$	$-\frac{(1-b)(1-d)}{4(1-bd)} + \frac{bd}{1-bd} \rho_L^{(1)}$
LD ( $\lambda > 1, \lambda > b$ )	$\frac{1-c\lambda}{(1+\lambda)^2}$	0	$-\frac{b(\lambda-d)-(1-d\lambda)}{(1+\lambda)^2}$	$\frac{b(\lambda-d)-(1-d\lambda)}{(1+\lambda)^2}$
HD ( $b > 1, b > \lambda$ )	$\frac{(b-c)(1-bc)\lambda}{(1+b)^2(1-c\lambda)}$	$\frac{(b-c)(1-b\lambda)}{(1+b)^2(1-c\lambda)}$	0	0

Table 1: Difference between boundary density and average bulk density in each phase. The value  $\rho_L^{(1)}$  in the MC phase is given in (5.5). Recall that  $-1 < c, d \leq 0$  in all phases.

In Table 1 we give the densities of species 1 and 2 at the first and last sites. We present these as the difference from the bulk density, i.e.  $\rho_i^{(j)} - \rho^{(j)}$ . Of note is that this density difference can change signs for both species at the right boundary in the LD phase, and for species 2 at the left boundary in the HD phase. We identify the following subphases:

- HD1:  $b > \lambda^{-1}, b > \lambda$ : Here  $\rho_1^{(2)} < \rho^{(2)}$ . A typical profile is shown in Figure 3(a).

- HD2:  $1 < b < \lambda^{-1}$ : Here  $\rho_1^{(2)} > \rho^{(2)}$ . A typical profile is shown in Figure 3(b).
- LD1:  $\frac{1-d\lambda}{\lambda-d} < b < \lambda$ : Here  $\rho_L^{(1)} < \rho^{(1)}$  and  $\rho_L^{(2)} > \rho^{(2)}$ . A typical profile is shown in Figure 3(c).
- LD2:  $\lambda > 1, b < \frac{1-d\lambda}{\lambda-d}$ : Here  $\rho_L^{(1)} > \rho^{(1)}$  and  $\rho_L^{(2)} < \rho^{(2)}$ . A typical profile is shown in Figure 3(d).



**Figure 6:** Division of phases according to the difference between bulk and boundary densities for a fixed value of  $d$ .

These subdivisions are depicted in Figure 6.

Beyond the density difference at the boundary, it would be interesting to calculate the correlation lengths, that is the form of the decay to the bulk density values. For the single species ASEP, this has been studied through a variety of different approaches [28, 29, 30, 1, 31, 27, 22].

We also note that the phase diagrams in Figures 5 and 6 resemble those that have appeared in other contexts in connection with the single species ASEP. The subdivisions of the high density phase in Figure 5 (related to the scaling of the density  $\rho_L^{(1)}$ ) appear in the phase diagram for the correlation lengths of the ASEP [27]. And the subdivisions in Figure 6 are similar (but not identical) to the parameter constraints for which there are finite dimensional representations of the matrix product algebra [32]. It would be interesting to know if any deeper connection exists in these cases.

## Acknowledgements

Our warm thanks go to Matthieu Vanicat and Luigi Cantini for discussions and suggestions. The first and third authors were partially supported by the UGC Centre for Advanced Studies. The first author acknowledges support from the Fondation Sciences Mathématiques de Paris for a visit to IHP and from DST grant DST/INT/SWD/VR/P-01/2014.

## References

- [1] B. Derrida, M. R. Evans, V. Hakim, and V. Pasquier, “Exact solution of a 1D asymmetric exclusion model using a matrix formulation,” *J. Phys. A: Math. Gen.* **26** no. 7, (1993) 1493.
- [2] M. J. Simpson, K. A. Landman, and B. D. Hughes, “Multi-species simple exclusion processes,” *Physica A* **388** no. 4, (2009) 399 – 406.
- [3] T. Chou, K. Mallick, and R. Zia, “Non-equilibrium statistical mechanics: from a paradigmatic model to biological transport,” *Rep. Prog. Phys.* **74** (2011) 116601, [arXiv:1110.1783](#) [`cond-mat.stat-mech`].
- [4] M. Bruna and S. J. Chapman, “Diffusion of multiple species with excluded-volume effects,” *J. Chem. Phys.* **137** (2012) 204116.
- [5] M. R. Evans, D. P. Foster, C. Godrèche, and D. Mukamel, “Asymmetric exclusion model with two species: Spontaneous symmetry breaking,” *J. Stat. Phys.* **80** no. 1, (1995) 69–102.
- [6] C. Arita, “Phase transitions in the two-species totally asymmetric exclusion process with open boundaries,” *J. Stat. Mech.* (2006) P12008.
- [7] A. Ayyer, J. L. Lebowitz, and E. R. Speer, “On the two species asymmetric exclusion process with semi-permeable boundaries,” *J. Stat. Phys.* **135** no. 5-6, (2009) 1009–1037, [arXiv:0807.2423](#) [`cond-mat.stat-mech`].
- [8] A. Ayyer, J. L. Lebowitz, and E. R. Speer, “On some classes of open two-species exclusion processes,” *Markov Processes and Related Fields* **18** no. 1, (2012) 157–176, [arXiv:1008.4721](#) [`cond-mat.stat-mech`].
- [9] M. Uchiyama, “Two-species asymmetric simple exclusion process with open boundaries,” *Chaos, Solitons & Fractals* **35** no. 2, (2008) 398 – 407.
- [10] N. Crampe, K. Mallick, E. Ragoucy, and M. Vanicat, “Open two-species exclusion processes with integrable boundaries,” *J. Phys. A: Math. Theor.* **48** no. 17, (2015) 175002, [arXiv:1412.5939](#) [`cond-mat.stat-mech`].
- [11] N. Crampe, M. R. Evans, K. Mallick, E. Ragoucy, and M. Vanicat, “Matrix product solution to a 2-species TASEP with open integrable boundaries,” *J. Phys. A: Math. Theor.* **49** no. 47, (2016) 475001, [arXiv:1606.08148](#) [`cond-mat.stat-mech`].
- [12] E. Duchi and G. Schaeffer, “A combinatorial approach to jumping particles,” *J. Combin. Theory Ser. A* **110** no. 1, (2005) 1–29.
- [13] S. Corteel, O. Mandelshtam, and L. Williams, “Combinatorics of the two-species ASEP and Koornwinder moments,” [arXiv:1510.05023](#) [`math.CO`].
- [14] O. Mandelshtam and X. Viennot, “Tableaux combinatorics of the two-species PASEP,” [arXiv:1506.01980](#) [`math.CO`].

- [15] L. Cantini, “Asymmetric simple exclusion process with open boundaries and Koornwinder polynomials,” *Ann. Henri Poincaré* **18** (2017) 1121–1151, [arXiv:1506.00284 \[math-ph\]](#).
- [16] N. Crampe, C. Finn, E. Ragoucy, and M. Vanicat, “Integrable boundary conditions for multi-species ASEP,” *J. Phys. A: Math. Theor.* **49** no. 37, (2016) 375201, [arXiv:1606.01018 \[math-ph\]](#).
- [17] R. A. Blythe, M. R. Evans, F. Colaiori, and F. H. L. Essler, “Exact solution of a partially asymmetric exclusion model using a deformed oscillator algebra,” *J. Phys. A: Math. Gen.* **33** no. 12, (2000) 2313.
- [18] J. de Gier, C. Finn, and M. Sorrell, “The relaxation rate of the reverse-biased asymmetric exclusion process,” *J. Phys. A: Math. Theor.* **44** (2011) 405002, [arXiv:1107.2744 \[cond-mat.stat-mech\]](#).
- [19] R. A. Blythe and M. R. Evans, “Nonequilibrium steady states of matrix-product form: a solver’s guide,” *J. Phys. A: Math. Theor.* **40** no. 46, (2007) R333, [arXiv:0706.1678 \[cond-mat.stat-mech\]](#).
- [20] S. Sandow, “Partially asymmetric exclusion process with open boundaries,” *Phys. Rev. E* **50** no. 4, (1994) 2660.
- [21] M. Uchiyama, T. Sasamoto, and M. Wadati, “Asymmetric simple exclusion process with open boundaries and Askey–Wilson polynomials,” *J. Phys. A: Math. Gen.* **37** (2004) 4985, [arXiv:cond-mat/0312457 \[cond-mat.stat-mech\]](#).
- [22] A. B. Kolomeisky, G. M. Schütz, E. B. Kolomeisky, and J. P. Straley, “Phase diagram of one-dimensional driven lattice gases with open boundaries,” *J. Phys. A: Math. Gen.* **31** (1998) 6911.
- [23] N. Crampe, E. Ragoucy, and M. Vanicat, “Integrable approach to simple exclusion processes with boundaries. Review and progress,” *J. Stat. Mech.* (2014) P11032, [arXiv:1408.5357 \[math-ph\]](#).
- [24] G. Gasper and M. Rahman, *Basic hypergeometric series*. Cambridge university press, 1990.
- [25] R. Koekoek, P. Lesky, and R. Swarttouw, *Hypergeometric Orthogonal Polynomials and Their  $q$ -Analogues*. Springer Monographs in Mathematics. Springer Berlin Heidelberg, 2010.
- [26] D. Bressoud, “A simple proof of Mehler’s formula for  $q$ -Hermite polynomials,” *Indiana Univ. Math. J.* **29** (1980) 577–580.
- [27] T. Sasamoto, “One-dimensional partially asymmetric simple exclusion process with open boundaries: orthogonal polynomials approach,” *J. Phys. A: Math. Gen.* **32** (1999) 7109.
- [28] J. Krug, “Boundary-induced phase transitions in driven diffusive systems,” *Phys. Rev. Lett.* **67** (1991) 1882–1885.

- [29] B. Derrida, E. Domany, and D. Mukamel, “An exact solution of a one-dimensional asymmetric exclusion model with open boundaries,” *J. Stat. Phys.* **69** no. 3-4, (1992) 667–687.
- [30] G. Schütz and E. Domany, “Phase transitions in an exactly soluble one-dimensional exclusion process,” *J. Stat. Phys.* **72** no. 1-2, (1993) 277–296, [arXiv:cond-mat/9303038](#).
- [31] F. H. L. Essler and V. Rittenberg, “Representations of the quadratic algebra and partially asymmetric diffusion with open boundaries,” *J. Phys. A: Math. Gen.* **29** (1996) 3375.
- [32] K. Mallick and S. Sandow, “Finite-dimensional representations of the quadratic algebra: Applications to the exclusion process,” *J. Phys. A: Math. Gen.* **30** (1997) 4513, [arXiv:cond-mat/9705152](#) [[cond-mat.stat-mech](#)].